ELSEVIER
Surface and Coatings Technology 120–121 (1999) 166–172
SURFACE & COATINGS TECHNOLOGY
www.elsevier.nl/locate/surfcoat

Structural analysis of $Ti_{1-x}Si_xN_y$ nanocomposite films prepared by reactive magnetron sputtering

F. Vaz [a,*], L. Rebouta [a], B. Almeida [a], P. Goudeau [b], J. Pacaud [b], J.P. Rivière [b], J. Bessa e Sousa [c]

[a] Dept. Física, Universidade do Minho, Campus de Azurém, 4810 Guimarães, Portugal
[b] Laboratoire de Métallurgie Physique, Université de Poitiers, 86960 Futuroscope, France
[c] Dept. Física, Universidade do Porto, 4100 Porto, Portugal

Abstract

In this paper, we report on the preparation of thin films resulting from additions of Si to TiN matrix, by r.f. reactive magnetron sputtering.

Results of X-ray diffraction (XRD) in both θ–2θ and α–2θ scans showed that a mixture of two phases is present, where the first is most likely fcc TiN. The higher lattice parameter of this phase, about 0.429 nm (0.424 nm for bulk TiN), could be explained by taking into account that a correction of the residual stress effect on peak positions might slightly decrease the value of the lattice parameter (around 1%). Regarding phase 2, and although the exact nature of its composition is more difficult to evaluate, we believe that it is also a cubic lattice consisting of Ti—Si—N, where the Si could be occupying Ti positions within the TiN lattice. This would explain the low value of the lattice parameter, which by assuming a cubic structure would be 0.418 nm. Concerning texture evolution, phase 1 revealed some variations in preferential growth, which changed from ⟨111⟩ for low Si additions to ⟨220⟩ at intermediate Si additions and finally to a weak ⟨200⟩ texture for large Si additions. A small amorphous region of silicon nitride for large Si additions was also observed.

Fourier analysis of XRD patterns showed a decrease in the size of grains for small Si additions when compared to that of TiN. For higher Si contents, only small changes were observed, although a decrease in grain size seems to be the main tendency. The grains are within the range of 4–6 nm. High-resolution transmission electron microscopy (HRTEM) on $Ti_{0.63}Si_{0.37}N_{1.12}$ confirmed this nanocrystalline nature of the grains, revealing grains with sizes of about 2–3 nm. © 1999 Elsevier Science S.A. All rights reserved.

Keywords: Grain size; Hard coatings; Texture; Titanium and silicon nitride

1. Introduction

Nanocomposite thin films consisting of both nano-size solid solutions and nano-size polycrystalline materials embedded in various amorphous matrix materials provide a great potential for future mechanical devices. The use of coated materials in engines, machines, tools and other wear-resistant components is steadily increasing and has achieved a high level of commercial success, compared to the common non-coated materials such as steel. In this respect, TiN and (Ti,M)N coatings, where M = B, C, Al, Cr, etc., are being widely investigated and used [1–7] mainly because of their good properties, in particular high hardness and good adhesion to common coated materials, which is normally steel in these cases.

Recently, several authors have focused their attention on the improvement of TiN properties by the addition of Si either by CVD [8–15] and PVD [16–19] deposition techniques. These films were characterized as being nanocomposites, consisting of cubic nanocrystallites of titanium nitride embedded in an amorphous matrix of silicon nitride (with a size of a few angstroms). These coatings were claimed to have an extremely high hardness, reaching values as high as 50 GPa, depending on the Si content and especially on the small grain sizes.

Furthermore, it is well known that most properties of thin films are influenced by certain factors such as crystalline structure and texture [1–20]. The knowledge

* Corresponding author. Tel.: +351-53-510151; fax: +351-53-678981.
E-mail address: fvaz@fisica.uminho.pt (F. Vaz)

0257-8972/99/$ – see front matter © 1999 Elsevier Science S.A. All rights reserved.
PII: S0257-8972(99)00450-8

and characterization of these parameters are of major importance in order to understand both the process involved in the preparation and the future behaviour of such coatings. A useful and powerful technique in this field is X-ray diffraction. Using different modes, this technique allows information on the growth direction of a film to be obtained (fibre texture), but also gives an insight into how they grow, i.e. average crystallite size, misorientation of textured grains, etc.

In the present paper, we report, first, on the preparation and characterization of samples within the (Ti,Si)N ternary system, by r.f. reactive magnetron sputtering, using high-purity Ti and Si targets and a constant substrate holder rotation of 4 rpm. The second part presents results on coating structure as a function of Si content, obtained by XRD using both the common θ–2θ scans and the α–2θ scans modes, together with HRTEM observation.

2. Experimental

2.1. Sample materials

The $Ti_{1-x}Si_xN_y$ samples were prepared by reactive r.f. magnetron sputtering in an Ar/N_2 gas mixture (constant substrate holder rotation of 4 rpm) from high-purity Ti and Si targets, onto polished high-speed steel (AISI M2) and single crystal silicon (100) substrates. The samples were prepared with a constant substrate temperature of 300°C and bias voltages ranging from −75 to +25 V. Prior to all depositions, a Ti adhesion layer of approximately 0.35 μm was deposited in every sample. The atomic composition of the as-deposited samples was measured by Rutherford backscattering spectrometry (RBS). An average number of five 'ball cratering' (BC) experiments were carried out in each sample in order to determine its thickness. Further detailed information regarding the deposition process can be found elsewhere [18].

2.2. Structural characterization

2.2.1. X-ray diffraction technique (XRD)

XRD diagrams have been recorded using a conventional Siemens D5000 diffractometer, working with a copper X-ray tube and a secondary graphite monochromator, which avoids parasitic intensities (fluorescence) of Fe and Cr atoms from steel substrates.

Two geometric configurations of measurement were used in the X-ray experiments. In the first one, known as the Bragg–Brentano θ–2θ scans, the diffraction vector $\boldsymbol{q}$ (or the normal to the diffracting planes) is normal to the surface of the sample. In this geometry, only the planes that are parallel to the surface will be in the Bragg position. This configuration allows phase characterization in the coating (peak position analysis). In this study, the angular range was 30–80°. The peak width at half maximum was also measured. Line broadening is generally attributed to both coherent diffracting domain size (related to grain size in the growth direction of the coating) and microstrains due to stacking faults, dislocations and point defects. Though a detailed deconvolution was not performed, we determined the average crystallite size (vertical coherence width) using Fourier analysis. Since, in our samples, only one first-order diffraction profile is usually available, the method introduced by Mignot and Rondot [21] was used, which is based on the analysis of a single X-ray profile. This method uses a hyperbolic law to describe the microstrain term $\bar{\varepsilon}_n^2 = C/n$, in which, n is the harmonic number of the Fourier coefficients.

In the second geometry, known as the $\alpha-2\theta$ geometry (asymmetric), the incident angle α is fixed to a particular value during the 2θ scan. The diffraction vector $\boldsymbol{q}$ has a misorientation of an angle Ψ with respect to the normal of the sample surface. The population of the diffracting objects in Bragg's position, θ_B, varies as a function of the angle α (or $\Psi = \alpha - \theta_B$). In this way, fibre texture phenomenon may be probed when plotting the maximum intensity of the considered diffraction peak as a function of Ψ. This measurement is similar to that of the rocking curve (the angular position 2θ of the detector is fixed to the Bragg angular position) but more precise because, in this last case, the shift of the diffraction peak position due to residual stresses, which varies with the angle Ψ, is not taken into account. The full width at half maximum (FWHM) of the resulting curves is a function of the 'mosaic structure' of textured grains, which is a slight misorientation present in the irradiated area of the sample, because each block (subgrain) of a typical 'mosaic crystal' successively comes into the reflecting position as the sample is rotated [22]. The half width at half maximum (HWHM) value indicates misorientation of textured grains with respect to the surface and thus indicates the fibre texture quality.

2.2.2. Transmission electron microscopy at high resolution (HRTEM)

Transmission electron microscopy (TEM), being one of the most important techniques of structural characterization, is very complementary to X-ray diffraction. With X-ray diffraction, an average over a large area of the sample (of about 1 cm^2) is performed. On the contrary, TEM allows diffraction over very small region (typically a few hundred nanometres) and the direct observation of the sample in image mode at atomic resolution. By combining both XRD and TEM results, a better understanding of the structure of the sample can be achieved.

Regarding the sample preparation for TEM observation, the microcleavage technique was used because of

the high residual stress level presented by these samples [23], which leads to the development of several cracks during the preparation of the samples by the usual procedure (the 'sandwich method' [24]). The micro-cleavage method consists of making small scratches on the sample and then collecting the pieces that come off. It is a clean and fairly easy method but cannot be applied on every material. Observations were performed in a JEOL JEM3010 with high-resolution capabilities. The accelerating voltage was fixed at 300 kV. The point resolution is 0.19 nm at Scherzer defocus.

3. Results and discussion

3.1. Chemical analysis

Table 1 presents a summary of the analysed coatings, together with grain size evaluation, thickness measurements, 'ball cratering' (BC) and the atomic composition, obtained by Rutherford backscatering spectrometry (RBS).

3.2. Structural analysis

XRD patterns obtained on the as-deposited samples by the θ–2θ scans mode are shown in Fig. 1, where three different samples represent each of the three different groups of growth situations. All these samples were deposited at a bias voltage of -50 V. The results reveal a mixture of two phases, which structure seem to be similar to that of TiN. The phase, referred to as phase 1, is a fcc-type structure, with a lattice parameter of about 0.429 nm, which is greater than that of bulk TiN (0.424 nm). Taking into account that a correction of the residual stress effect on peak positions might slightly decrease the value of the lattice parameter (around 1%) [25], we believe that this phase can be assigned to the bulk TiN. For this phase, and concerning the texture evolution as a function of the Si content, a $\langle 111 \rangle$ preferential growth is visible for the samples with the lowest Si content (2.5 at.%), which is very similar to that of pure TiN (lower diagram in Fig. 1), also deposited in the rotation mode. Samples with intermediate Si contents (5.9, 7.4 and 10.6 at.%) show a $\langle 220 \rangle$ texture,

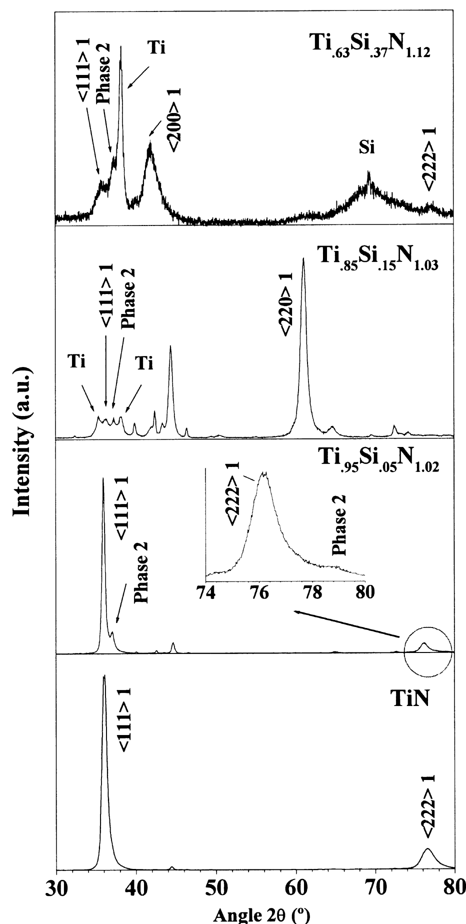

Fig. 1. Evolution of the θ–2θ diffraction diagrams (CuKα) measured on $Ti_xSi_{1-x}N_y$ coatings deposited on steel substrates as a function of Si content.

while with those with the highest Si content (17.5 at.%), a weak $\langle 200 \rangle$ texture was obtained.

The exact nature of the phase referred to as phase 2, is more difficult to evaluate since, in most cases, only one peak ($2\theta \approx 37.2°$) is clearly visible. Evidence of another peak is also visible when phase 2 is the only one that grows. For the cases where the two-phase mixture is present and phase 1 grows on the $\langle 200 \rangle$ direction, the diffraction peaks are very broad (FWHM $\approx 2°$), and so the observation of that second peak is very difficult (it appears very close to that of

Table 1
Thickness, composition and grain size of the samples

Composition	Ti (at.%)	Si (at.%)	N (at.%)	Thickness (μm)	Grain size (nm)
TiN	50	–	50	3.3	7
$Ti_{0.95}Si_{0.05}N_{1.02}$	47	2.5	50.5	1.6	8
$Ti_{0.88}Si_{0.12}N_{1.04}$	43.1	5.9	51	1.2	5
$Ti_{0.85}Si_{0.15}N_{1.03}$	41.9	7.4	50.7	2.1	6
$Ti_{0.78}Si_{0.22}N_{1.07}$	37.7	10.6	51.7	2.0	4
$Ti_{0.63}Si_{0.37}N_{1.12}$	29.7	17.5	52.8	1.9	5

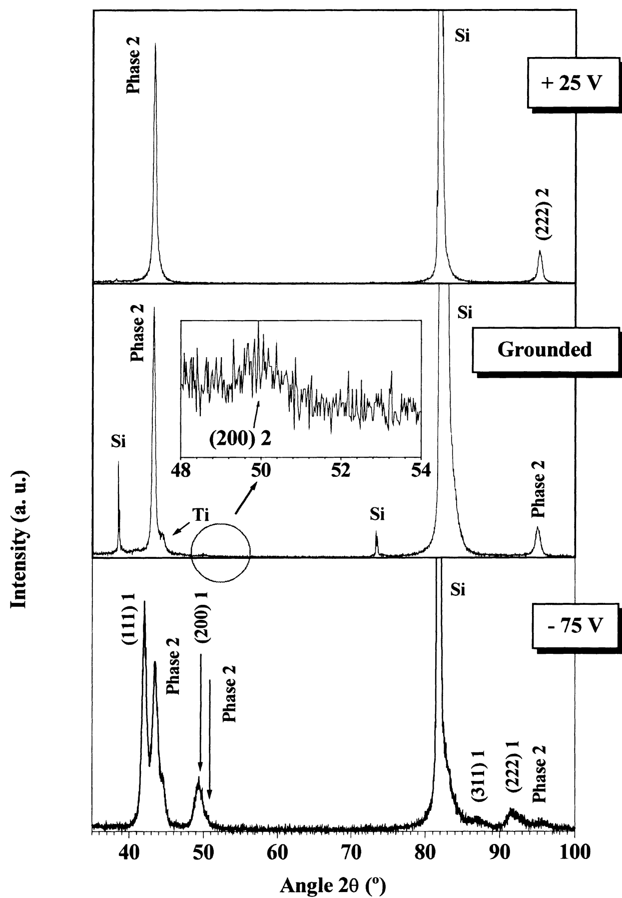

Fig. 2. θ–2θ diffraction diagrams (CoKα) recorded in $Ti_{0.80}Si_{0.20}N_{1.07}$, $Ti_{0.83}Si_{0.17}N_{1.07}$ and $Ti_{0.87}Si_{0.13}N_{1.04}$ samples.

⟨200⟩ from phase 1, at the right side tail — top diagram in Fig. 1). θ–2θ scans recorded in samples prepared with different substrate bias (+25 V — $Ti_{0.80}Si_{0.20}N_{1.06}$; grounded — $Ti_{0.83}Si_{0.17}N_{1.06}$ and −75 V — $Ti_{0.87}Si_{0.13}N_{1.04}$), using a Cobalt source (Fig. 2) revealed the presence of the two phases and, in particular, the second peak from phase 2. From this figure, the two distinct structures are clearly visible, where the so-called phase 2 would be formed under conditions where no ion bombardment of the growing film is present.

Although this behaviour might seem slightly difficult to interpret since it is somewhat in contradiction with the results published by other authors in this field [10–15,17,19], the same behaviour was also found in recent work developed in our laboratory, which is being carried out to study the influence of Al additions to (Ti,Si)N matrix [26]. According to this work, the mixture of the two phases was again observed and, in one sample where only reflections correspondent to phase 2 are present, the two stated peaks and another peak at $2\theta \approx 62.8°$ were clearly visible.

From the JCPDFS available data, it seems difficult to match this phase 2 with known compounds formed by the Ti, Si and N elements, (crystalline Si_3N_4 or from various phases of titanium silicide, Table 2). Anyway, from peak positions and considering that it would be highly improbable that this phase is a silicide (the cases where only phase 2 is present clearly exclude this possibility because of the total amount of nitrogen in the samples), we believe that it might be a cubic titanium silicon nitrogen phase, Ti—Si—N, where the Si could be occupying Ti positions in the cubic lattice of TiN. This configuration would explain the low value of the lattice parameter, which would be approximately 0.418 nm in this case. Assuming a cubic configuration and considering that the first peak would be the ⟨111⟩, the ⟨200⟩ would appear with $d=0.2091$ nm (0.2088 nm in the present case) and the ⟨220⟩ for $d=0.1479$ nm (0.1478 nm in the present case), which seem to correlate well with the obtained results. No evidence of significant changes in texture was observed for this phase.

The results using different bias voltages as well as different deposition rates (different powers applied to the targets) seem to indicate that the appearance of the observed phase mixture is most likely a consequence of the depositing species mobility, which is thought to promote some particular growth direction and atom arrangement [27]. Although the mixture of phases can be evidenced in all samples that were prepared under ion bombardment of the growing film, it seems that it is much clearer for the cases where phase 1 grows in the ⟨111⟩ orientation as well as in the cases where the deposition rate is low (typical values for deposition rates in our cases are 0.2 μm/h).

In order to investigate the fibre texture, α–2θ scan results on the ⟨111⟩ ($Ti_{0.95}Si_{0.05}N_{1.02}$) and (220)

Table 2
Plane, ⟨hkl⟩, and plane spacing, d (Å), for several materials containing Si (JCPDF database). The two closest reflections were chosen according to each reflection of phase 2 (the most intense reflections in this database are shown in bold)

Phase 2	Si_3N_4(Hex.)	Ti_5Si_4 (Tetra.)	Ti_5Si_3 (Hex.)	TiSi(Orth.)	$TiSi_2$(Orth.)
2.415	2.538 ⟨210⟩	**2.415 ⟨213⟩**	2.436 ⟨210⟩	**2.435 ⟨210⟩**	2.972 ⟨220⟩
	2.313 ⟨211⟩	2.373 ⟨220⟩	2.388 ⟨102⟩	2.335 ⟨102⟩	2.349 ⟨131⟩
2.088	2.155 ⟨202⟩	2.090 ⟨311⟩	2.116 ⟨112⟩	2.189 ⟨211⟩	2.093 ⟨022⟩
	2.080 ⟨301⟩	2.049 ⟨223⟩	2.011 ⟨202⟩	2.000 ⟨301⟩	2.067 ⟨400⟩
1.478	1.486 ⟨202⟩	1.502 ⟨420⟩	1.479 ⟨320⟩	1.150 ⟨223⟩	1.486 ⟨440⟩
	1.437 ⟨301⟩	1.468 ⟨316⟩	1.468 ⟨312⟩	1.137 ⟨230⟩	1.470 ⟨422⟩

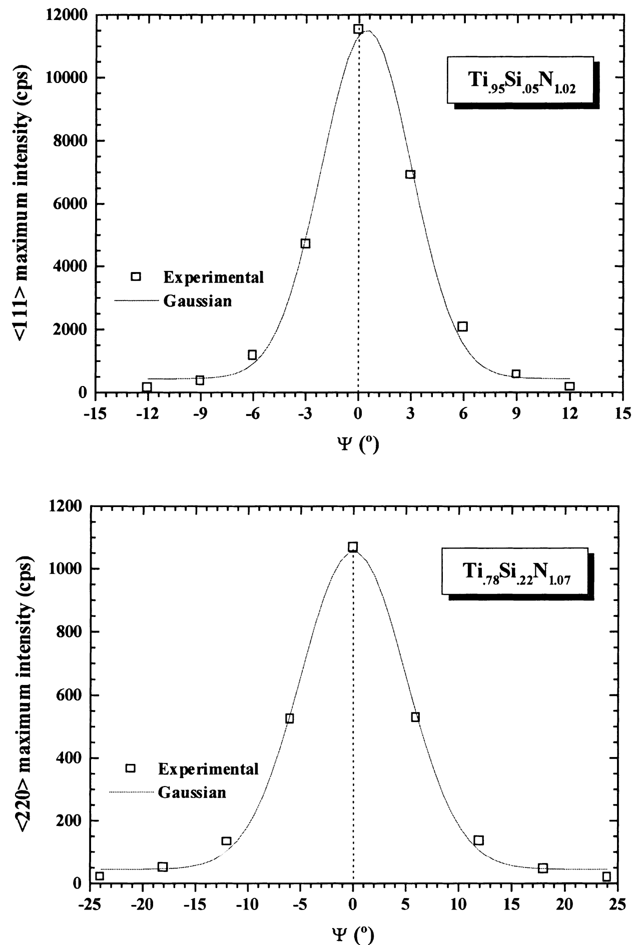

Fig. 3. Rocking curves deduced from detector scans measurements performed on samples showing (a) ⟨111⟩ and (b) ⟨220⟩ texture.

($Ti_{0.78}Si_{0.22}N_{1.0}$) diffraction peaks from phase 1 are shown in Fig. 3. The experimental points of each curve were fitted using a Gaussian. The maximum intensity value corresponding to the maximum of the curve (θ–2θ) is higher for the ⟨111⟩ surface compared to the (220) (factor 10), although the ratio of the structure factors (F_{111}/F_{220}) is equal to 1.6. This difference may be attributed to the form factor, which is linked with the size of diffracting grains (factor 2), and the quality of the texture. In this last case, the FWHM is equal to 7° (misorientation of $\pm 3.5°$) and 12° ($\pm 6°$) for ⟨111⟩ and ⟨220⟩ textures, respectively. Concerning the third group of samples, which correspond to a weak ⟨200⟩ texture in phase 1, we can say that this growth is typically random since the width of the rocking curve is extremely high.

TEM observations (high resolution) carried out on samples in group 2 (intermediate Si content) and 3 (high Si content) correlate very well with the X-ray diffraction measurements but also provide new information. Experiments on $Ti_{0.63}Si_{0.37}N_{1.12}$ (Fig. 4) have confirmed the nanocrystalline nature of the grains. A closer look at this picture reveals that small crystallites with a size of between 2 and 3 nm can easily be observed. The dispersion of the grain size distribution is very small. In the diffraction mode, these grains were identified as the TiN nanocrystalline phase in the diffraction mode. Also from the observation of this figure, an amorphous region can be distinguished, which we attribute to an amorphous silicon nitride phase. This formation of an amorphous region for a certain critical thickness of the pseudomorphic material (supposed Ti—Si—N in our case) might be explained based on the assumption that the seed material (TiN) is no longer sufficient to induce that crystalline growth. In addition, the low solubility of the Si in TiN acts in the same direction. The possible presence of Si between grains could be correlated with the fact that the Ti—Si—N lattice parameter deduced from X-ray measurements does not change (decrease) with increasing Si contents.

Finally, it is important to note that the resolution of the electron diffraction method is weaker than that of X-ray diffraction and thus cannot show the two phase mixture clearly. In some regions of Fig. 4, a different kind of grains seems to be present, although its association with phase 2 might be a little precipitate. In order to better clarify the existence of this phase mixture, HRTEM experiments are being performed on one of the samples where only phase 2 is present as well in another sample where the two-phase mixture is very clear (the two samples referred to in Fig. 2).

Regarding grain size evolution and in spite of the high level of Si addition present in $Ti_{0.63}Si_{0.37}N_{1.12}$, the grains are extremely small with values that lie within the range of 2–3 nm. This fact reveals a different behaviour from that stated by Veprek et al. [10–15]. These authors observed a minimum in grain size for Si contents between 5 and 7 at.%, followed by a significant increase at higher contents.

The values of grain size observed by electron microscopy (in plane) are very similar to those obtained by the Fourier coefficients in the θ–2θ measurements (in depth), which may indicate that the grains might be fairly spherical and with little dispersion.

4. Conclusions

Thin films within the (Ti,Si)N ternary system were prepared by reactive magnetron sputtering. The X-ray technique, in both the θ–2θ and α–2θ scan modes, was successfully used for phase and texture characterization and enabled conclusions to be drawn about the formation of a mixture of two phases in that (Ti,Si)N system.

These structural studies have clearly shown that coatings are principally composed of a two-phase mixture with a structure similar to that of TiN. A lattice parameter of about 0.429 nm was deduced for phase 1 — TiN.

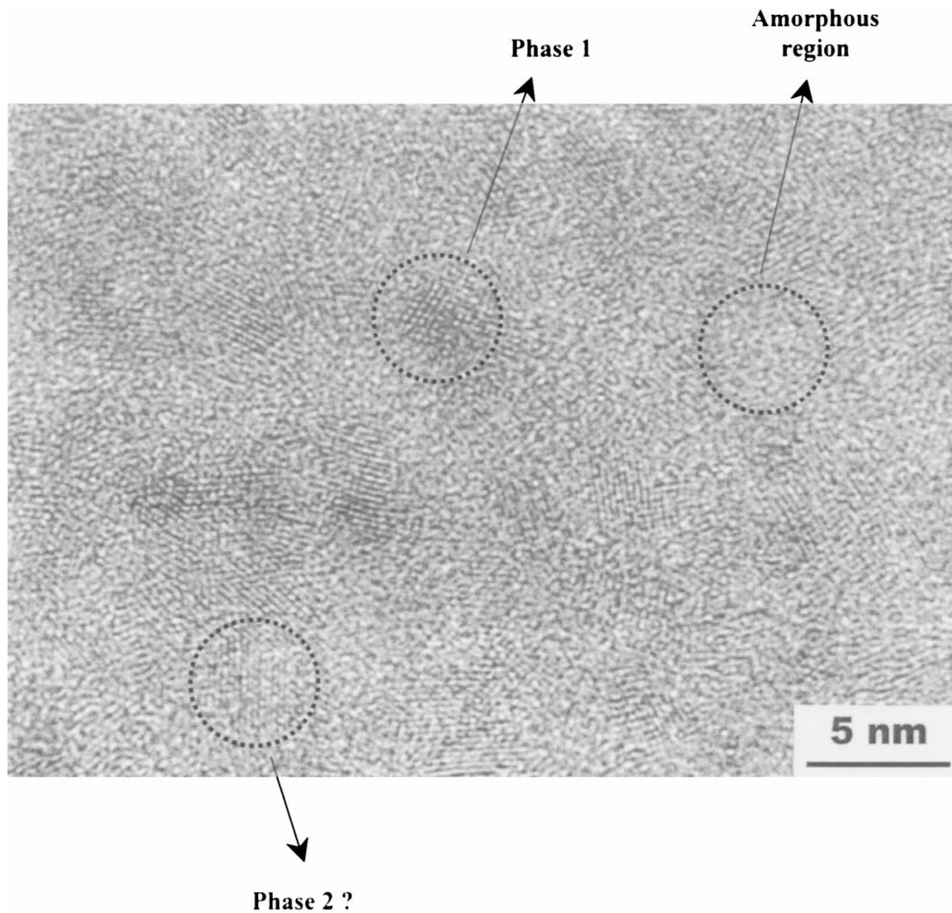

Fig. 4. HRTEM observation in $Ti_{0.63}Si_{0.37}N1_{0.12}$ coatings.

Regarding phase 2, the association with any known compound formed with Ti and Si is very difficult to achieve. Following the obtained XRD patterns, it seems that it can be a cubic lattice, where the Si in this case would be occupying some of the Ti positions. A lattice parameter of about 0.418 nm (Ti—Si—N) would result from this assumption. Fourier analysis on the diffraction patterns revealed a nanocrystalline nature of the developed grains (4–6 nm), confirmed by HRTEM micrographs, which reveal crystallites with a size of between 2 and 3 nm. This mixture of phases has been found to be closely related to the applied substrate bias, since phase 2 was the only phase observed under conditions where no bombardment of the growing film was present. This conclusion enabled the assumption that phase 2 is the one that appears without substrate bombardment, and that is partially transformed into 'pure' TiN phase as a result of ion bombardment of the growing film.

HRTEM experiments have shown that when the Si content is high, a small amorphous region develops between grains, which could be attributed to silicon nitride (Si_3N_4). Nevertheless, all these hypotheses need further experiments. Extended X-ray absorption fine structure analyses on K—Ti and K—Si absorption edge experiments, which have been accepted at LURE, the French synchrotron radiation facility (Orsay), will be carried out in the near future.

Acknowledgements

The authors gratefully acknowledge the financial support of the 'Fundação para a Ciência e Tecnologia' (FCT) during the course of this research under project n PBICT/P/CTM/1962/95 and also the French CNRS Institution and the Portugese ICCTI Institution through CNRS/ICCTI Programs (N: 5522-1998 and 7087-1999).

References

[1] O. Knotek, W.D. Münz, T. Leyendecker, J. Vac. Sci. Technol. A 5 (4) (1987) 2173.
[2] O. Knotek, M. Bohmer, T. Leyendecker, F. Jungblut, Mater. Sci. Eng. A 105–106 (1988) 481.
[3] H. Freller, H. Haessler, Surf. Coat. Technol. 36 (1988) 219.
[4] Y.I. Chen, J.G. Duh, Surf. Coat. Technol. 48 (1991) 163.

[5] V.R. Parameswaran, J.-P. Immarigeon, D. Nagy, Surf. Coat. Technol. 52 (1992) 251.
[6] F. Hohl, H.-R. Stock, P. Mayr, Surf. Coat. Technol. 54–55 (1992) 160.
[7] J.G. Duh, J.C. Doong, Surf. Coat. Technol. 56 (1993) 257.
[8] T. Hirai, S. Hayashi, J. Mater. Sci. 17 (1982) 1320.
[9] L. Shizhi, S. Yulong, P. Hongrui, Plasma Chem. Plasma Process. 12 (3) (1992) 287.
[10] S. Veprek, S. Reiprich, L. Shizhi, Appl. Phys. Lett. 66 (1995) 2640.
[11] S. Veprek, S. Reiprich, Thin Solid Films 268 (1995) 64.
[12] S. Veprek, M. Haussmann, S. Reiprich, J. Vac. Sci. Technol. A 14 (1996) 46.
[13] S. Veprek, Surf. Coat. Technol. 97 (1997) 15.
[14] S. Veprek, P. Nesládek, A. Niederhofer, F. Glatz, M. Jílek, M. Šíma, Surf. Coat. Technol. 108–109 (1998) 138.
[15] S. Veprek, Thin Solid Films 317 (1998) 449.
[16] L. Rebouta, F. Vaz, M. Andritschky, M.F. Silva, Surf. Coat. Technol. 76–77 (1995) 70.
[17] X. Sun, J. Reid, E. Kolawa, M.-A. Nicolet, R. Ruiz, J. Appl. Phys. 81 (2) (1997) 664.
[18] F. Vaz, L. Rebouta, S. Ramos, M.F. da Silva, J.C. Soares, Surf. Coat. Technol. 108–109 (1998) 236.
[19] M. Diserens, J. Patscheider, F. Levy, Surf. Coat. Technol. 108–109 (1998) 241–246.
[20] P. Gergaud, S. Labat, O. Thomas, Thin Solid Films 319 (1998) 9–15.
[21] J. Mignot, S. Rondot, Acta Metallurg. 23 (1975) 1321.
[22] B.D. Cullity, Elements of X-ray Diffraction, second ed. Addison-Wesley, Menlo Park, CA, 1978.
[23] F. Vaz, L. Rebouta, R.M.C. da Silva, M.F. da Silva, J.C. Soares, Vacuum 52 (1999) 209–214.
[24] L. Feldman, J. Mayer, in: Fundamentals of Surface and Thin Film Analysis, Elsevier Science, Amesterdam, 1986, p. 179.
[25] R.C. Cammarata, R.K. Eby, J. Mater. Res. 5 (1991) 888.
[26] L. Rebouta, F. Vaz, S. Carvalho, to be published.
[27] D.N. Lee, J. Mater. Sci. 24 (1989) 4375–4378.